

# Numerical Simulation of H<sub>2</sub>/Air Detonation Using Detailed Reaction Models

Fumiya Togashi\*, Rainald Löhner†

*School of Computational Sciences,*

*George Mason University, Fairfax, VA 22030, USA*

and

Nobuyuki Tsuboi‡

*Institute of Space and Astronautical Science,*

*Japan Aerospace Exploration Agency, Yoshinodai 3-1-1, 229-8510, Japan*

## Abstract

A code to simulate chemically reacting flows has been developed. The code considers a detailed chemical reaction model and proper schemes were adopted to treat the chemical reactions. The code was tested and validated against a series of 1-D experiments with several chemical reaction models. The core subroutines developed under this study were incorporated into FEFLO. FEFLO with chemical reaction model was tested with 1-D computation of detonation, and 3-D computation of detonation propagating in a tube with a spiral obstacle was conducted.

## Introduction

A detonation is a shock wave sustained by the energy released by combustion. The typical case is an explosion. For over hundred twenty years, various experiments and calculations of this phenomenon have been done because the analysis of the nature and structure of a detonation is very significant from the point of safety engineering. These results, especially concerning the experimental data, are very useful even for the current study.

Recently, detonation has been applied to the next generation engines such as Pulse Detonation Engine (PDE) and Supersonic Combustion Ram Jet engine (SCRAM Jet) [1, 2]. On the other hand, a detonation of the type

---

\* Research Associate, School of Computational Sciences, George Mason University, 4400 University Drive, MS 4C7, AIAA Member

† Professor, School of Computational Sciences, George Mason University, 4400 University Drive, MS 4C7, AIAA Member

‡ Associate Professor, Space Transportation Engineering Department, Institute of Space and Astronautical Science, Japan Aerospace Exploration Agency, Yoshinodai 3-1-1, 229-8510, Japan, AIAA member

considered here can also be applied to some fuel-air explosives. In order to understand the nature and structure of a detonation under these various situations, more analysis of a detonation under various circumstances is required. Especially, the development of proper numerical analysis tools is necessary to enhance understanding and reduce cost and risk. Numerical simulation of these flow fields is not an easy task because the computation includes complicated combustion kinetics, diffusion processes, and huge energy releases into the field and requires much more nodal points compared to inert compressible flow computations. However, due to the recent progress in both computational methods and available computer facilities, the computation with detailed reaction models has been possible, though it is limited to smaller spatial domains [3-9].

One of the famous detailed reaction models is the Jachimowski model proposed in 1988 [10]. In some papers, this model was modified and adopted for hypersonic combustion computations [5, 11]. On the other hand, in 1999 Petersen and Hanson proposed another detailed chemical reaction model (PH model) [12]. Tsuboi *et al.* examined the validity of some detailed chemical reaction models including Jachimowski model and PH model. In their study, they concluded that the PH model shows better results at extremely high pressure regions while the Jachimowski model also shows good results.

The motivation of this study is to construct a numerical code coupled to the PH model and to verify the new code. The newly constructed code is applied to 1-D and 3-D computations of detonation. Then the new code is applied to a 3-D computation of detonation propagation in a tube with a spiral obstacle.

## Reaction Model and Governing equations

In this study, the Petersen & Hanson model (PH model) is used for chemical kinetics that consists of 9 species ( $H_2$ ,  $O_2$ ,  $H$ ,  $O$ ,  $OH$ ,  $HO_2$ ,  $H_2O_2$ ,  $H_2O$ , and  $N_2$ ) and 18 elementary reactions. The data for the chemical reaction was taken from the paper of Petersen & Hanson [12], and is reproduced in detail in Appendix 1. This model was proposed by Petersen and Hanson as a new detailed chemical reaction model to solve detonation problems. The model has the feature that the pressure dependence on a forward reaction coefficient is included in the collision reaction with a third body. Namely,  $HO_2$  and  $H_2O_2$  chemistry near the second and third explosion limits are introduced that are necessary for ignition at extremely high pressure but are lacking for some finite rate chemical models currently in use.

The production rate of each chemical species,  $\dot{\omega}_s$  is given by combining the elementary chemical reactions in the kinetic model as follows:

$$\dot{\omega}_s = M_s \sum_{j=1}^{N_r} \left( \sum_{l=1}^n \alpha_{lj} C_l \right)^{\beta_j} (\gamma_{js}'' - \gamma_{js}') \left[ K_{fj} \prod_{i=1}^{N_s} C_i^{\gamma_{ji}'} - K_{bj} \prod_{i=1}^{N_s} C_i^{\gamma_{ji}''} \right] \quad (1)$$

where  $M_s$  denotes the molecular weight of species  $s$ ,  $C_s$  denotes the mole fraction,  $\alpha$  is a third body

coefficient, and  $\gamma''_{js}$  and  $\gamma'_{js}$  are the stoichiometric coefficients.  $K_f$  and  $K_b$  are the forward and backward rate constants derived from an Arrhenius form as follows:

$$K(T) = A \exp(-E / RT) \quad (2)$$

The governing equations are the Euler equations and solved by an explicit method. As an approximate Riemann solver, the AUSM-DV scheme is employed. High-order flux reconstruction is carried out via a MUSCL scheme. The flux limiter proposed by Shuen [13] was adopted. The source term of the chemical reaction was treated in a linearly point-implicit manner.

The governing equations can be written as follows:

$$\frac{\partial \mathbf{Q}}{\partial t} + \frac{\partial \mathbf{E}}{\partial x} = \mathbf{S} \quad (3)$$

$$\mathbf{Q} = \begin{bmatrix} \rho \\ \rho u \\ \rho e \\ \rho_l \end{bmatrix}, \mathbf{E} = \begin{bmatrix} \rho u \\ \rho u^2 + p \\ (\rho e + p)u \\ \rho_l u \end{bmatrix}, \mathbf{S} = \begin{bmatrix} 0 \\ 0 \\ 0 \\ \omega_l \end{bmatrix} \quad (4)$$

The source term of the chemical reaction  $\mathbf{S}$  is treated implicitly as follows:

$$\frac{\partial \mathbf{Q}}{\partial t} + \frac{\partial \mathbf{E}}{\partial x} \Big|^{n+1} = \mathbf{S}^{n+1} + (1 - \theta) \mathbf{S}^n \quad (5)$$

$\mathbf{S}^{n+1}$  is written as:

$$\mathbf{S}^{n+1} = \mathbf{S}^n + \frac{\partial \mathbf{S}}{\partial \mathbf{Q}} \Big|^{n+1} \Delta \mathbf{Q} + \mathbf{O}((\Delta t)^2), \quad (6)$$

resulting in:

$$\frac{\partial \mathbf{Q}}{\partial t} + \frac{\partial \mathbf{E}}{\partial x} \Big|^{n+1} = \frac{\Delta \mathbf{Q}}{\Delta t} + \frac{\partial \mathbf{E}}{\partial x} \Big|^{n+1} = \mathbf{S}^n + \theta \frac{\partial \mathbf{S}}{\partial \mathbf{Q}} \Big|^{n+1} \Delta \mathbf{Q} \quad (7)$$

or:

$$\left( \mathbf{I} - \theta \Delta t \frac{\partial \mathbf{S}}{\partial \mathbf{Q}} \right)^n \Delta \mathbf{Q} = -\Delta t \left( \frac{\partial \mathbf{E}}{\partial \mathbf{x}} - \mathbf{S} \right)^n \quad (8)$$

This may be written as:

$$D \Delta \mathbf{Q} = RHS^n \quad (9)$$

$$D = \mathbf{I} - \theta \Delta t \frac{\partial \mathbf{S}}{\partial \mathbf{Q}} \Big|_n, \quad RHS^n = -\Delta t \left( \frac{\partial \mathbf{E}}{\partial \mathbf{x}} - \mathbf{S} \right)^n \quad (10)$$

D is a coefficient matrix of  $\Delta \mathbf{Q}$ .  $RHS^n$  denotes the right hand side at time n.  $RHS^n$  can be divided into two terms.  $RHS_1^n$  denotes the term of flow variables and  $RHS_2^n$  is the term of chemical reactions as follows:

$$D = \begin{bmatrix} I & 0 \\ D_{21} & D_{22} \end{bmatrix}, \quad RHS^n = \begin{bmatrix} RHS_1^n \\ RHS_2^n \end{bmatrix} \quad (11)$$

$$\begin{bmatrix} I & 0 \\ D_{21} & D_{22} \end{bmatrix} \Delta \mathbf{Q} = \begin{bmatrix} I & 0 \\ D_{21} & D_{22} \end{bmatrix} \begin{bmatrix} \Delta \mathbf{Q}_1 \\ \Delta \mathbf{Q}_2 \end{bmatrix} = \begin{bmatrix} RHS_1^n \\ RHS_2^n \end{bmatrix} \quad (12)$$

Unknown  $\Delta \mathbf{Q}$  is obtained from above calculations as follows:

$$\Delta \mathbf{Q}_1 = RHS_1^n \quad (13)$$

$$\Delta \mathbf{Q}_2 = (D_{22})^{-1} (RHS_2^n - D_{21} RHS_1^n) \quad (14)$$

Matrix inversion of  $D_{22}$  is not necessary for steady computations. Some effective diagonal algorithm methods were developed [14, 15]. Concerning unsteady flow computations, however, the matrix inversion is necessary for an accurate computation.

## Comparison with Experimental data

To verify the code, the ignition delay time behind the reflected shock for stoichiometric hydrogen-air mixtures near the second explosion limit was computed and compared with experimental data (Fig. 1). This comparison is often used for the verification of chemical reaction code. The data for the comparison included the ignition delay data at pressures of 0.5, 1.0, and 2.0 atm [10]. PH model, modified Jachimowski model [5,

11], and the Stahl-Warnatz model (SW model) [16] were compared with experimental data.

At this comparison, the SW model showed relatively large ignition delay time. Concerning the other two models, they showed similar results in the high temperature region. However, at lower temperatures, the Jachimowski model showed a relatively short ignition delay time. The PH model showed good agreement with experimental data through three different pressure comparisons.

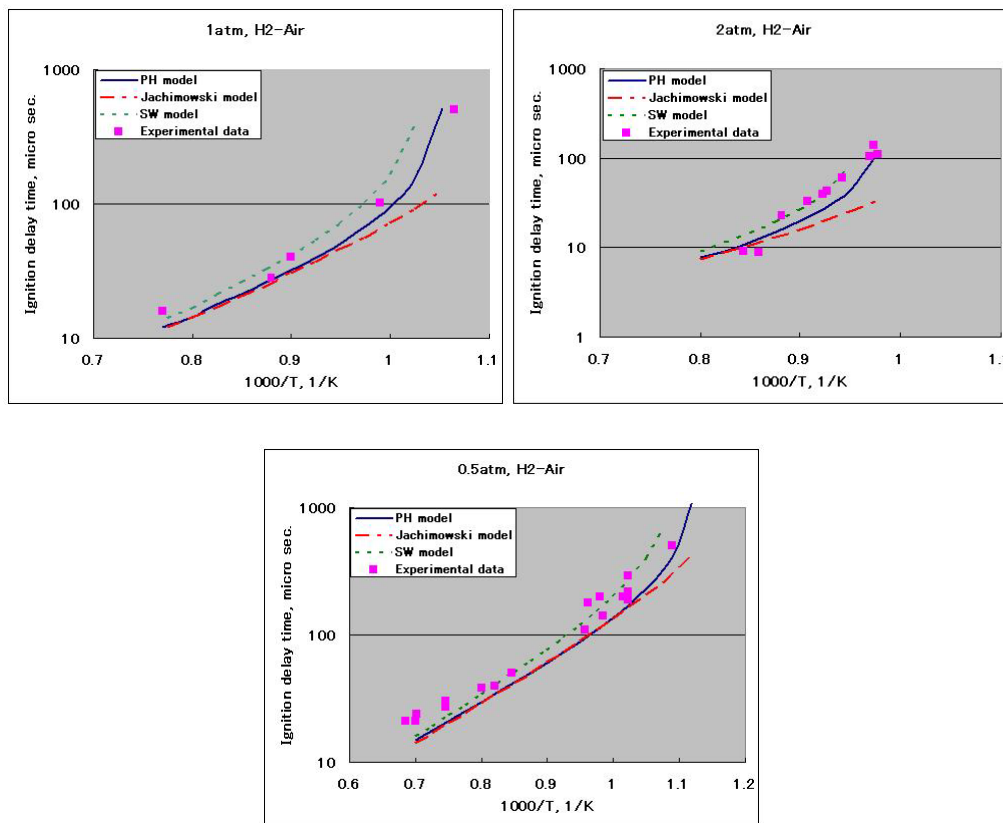


**Fig. 1 Ignition delay time, H<sub>2</sub>-Air mixture**

### 1-D Computation of Detonation

A 1-D detonation flow was computed for demonstrating the new code. The initial conditions are composed of two regions, separated at  $x = 0.005$  m. The initial condition of high pressure region was 38atm, 1420K, and that of low pressure region was 1atm and 300 K. In the whole domain, the mole concentration ratio of the H<sub>2</sub>/O<sub>2</sub>/N<sub>2</sub> gas mixture was 2:1:3.76. The mesh size was 5 $\mu$ m. The computations were conducted with spatially 2<sup>nd</sup> order scheme and 1<sup>st</sup> order scheme. Figure 2 and 3 show the pressure and temperature profiles at various times. In Fig. 2 and 3, it was observed that the high pressure region was ignited at about 4.5  $\mu$ sec. Then, the reaction zone caught up the shock front and the detonation was initiated at about 11.2  $\mu$ sec. The velocity of the

shock front was accelerated to over 2500 m/s during the detonation initiation process. This overdriven detonation converged to the CJ detonation velocity at around 36  $\mu$ sec. There were no large differences between the 2<sup>nd</sup> order scheme and 1<sup>st</sup> order scheme concerning the average pressure, temperature, and detonation velocity. However, the fluctuation of the detonation front was only observed from the results of 2<sup>nd</sup> order scheme in Fig. 2-b and Fig. 3-b.

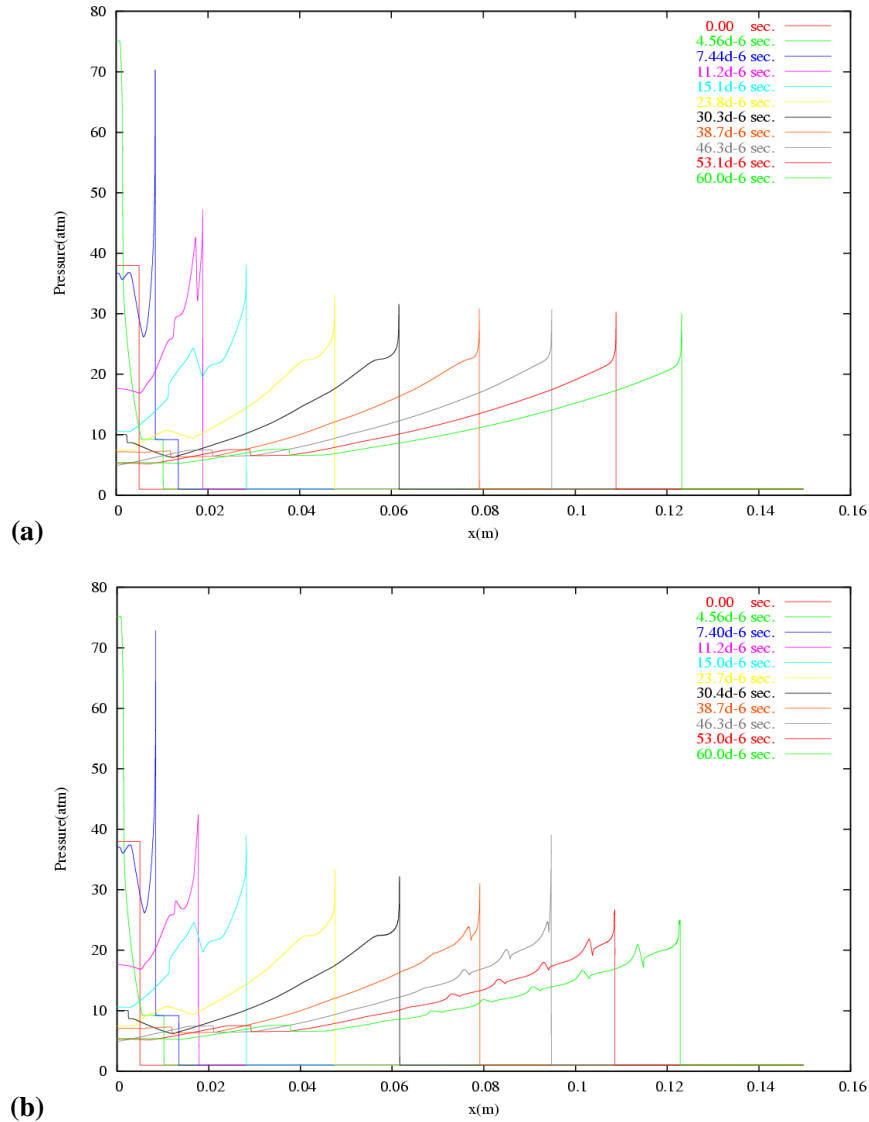


**Fig. 2 Pressure profiles at various times (a) spatially 1<sup>st</sup> order scheme (b) spatially 2<sup>nd</sup> order scheme**

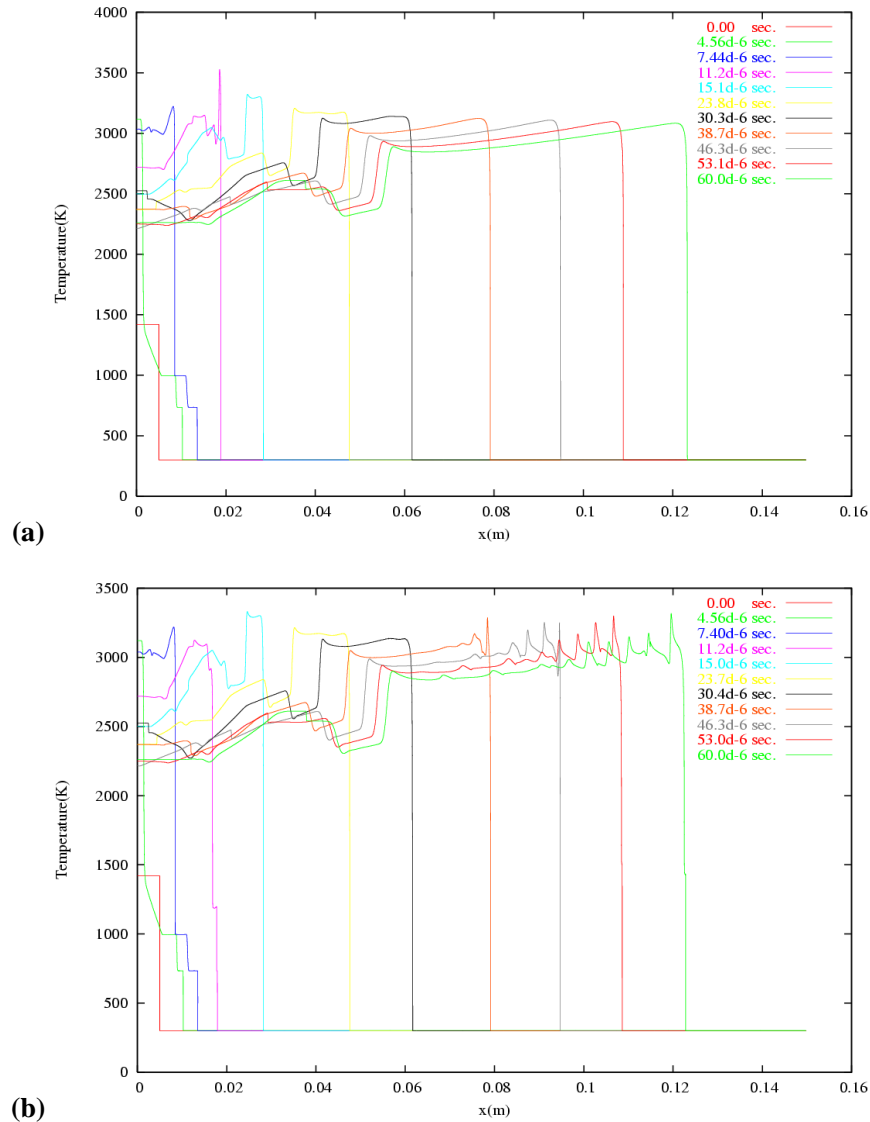


**Fig. 3 Temperature profiles at various times (a) spatially 1<sup>st</sup> order scheme (b) spatially 2<sup>nd</sup> order scheme**

### 3-D Flow Solver

The 1-D solver described in the previous section was implemented into FEFLO, a general-purpose CFD code based on the following general principles:

- Use of unstructured grids (automatic grid generation and mesh refinement);
- Finite element discretization of space;
- Separate flow modules for compressible and incompressible flows;
- ALE formulation for body fitted moving grids;
- Embedded formulation for complex/dirty geometries;
- Edge-based data structures for speed;
- Optimal data structures for different supercomputer architectures;

- Bottom-up coding from the subroutine level to assure an open-ended, expandable architecture.

The code has had a long history of relevant applications [17-25]. Over the last three years, FEFLO has been ported to both shared memory [26-28] and distributed memory [19, 29, and 30] machines.

The spatial approximation is accomplished via the Galerkin weighted residual method. The unknown vector  $\mathbf{u}$  is approximated by a set of shape-functions:

$$\mathbf{u} \approx N^i \mathbf{u}_i^h \quad (15)$$

where  $N^i$  denotes the shape function associated with node  $i$  and  $\mathbf{u}_i^h$  the numerical value of  $\mathbf{u}$  at node  $i$ .

Weighing Eqn. (15) with the available set of shape-function  $N^i$  leads to:

$$\int_{\Omega} N^i (\mathbf{u}_{,t}^h + \nabla \cdot \mathbf{F}) d\Omega = 0 \Rightarrow \int_{\Omega} N^i [N^i (\hat{\mathbf{u}}_j)_{,t} + \nabla \cdot \mathbf{F}(N^i \hat{\mathbf{u}}_j)] d\Omega = 0 \quad (16)$$

In order to simplify the algebra involved (and CPU), one may use, without noticeable deterioration of results:

$$\mathbf{F}(N^j \hat{\mathbf{u}}_j) = N^j \mathbf{F}(\hat{\mathbf{u}}_j) \quad (17)$$

which then translates into:

$$\int_{\Omega} N^i N^j d\Omega (\hat{\mathbf{u}}_j)_{,t} + \int_{\Omega} N^i \nabla \cdot N^j d\Omega \mathbf{F}(\hat{\mathbf{u}}_j) = 0 \quad (18)$$

or

$$\mathbf{M}_c \cdot \hat{\mathbf{u}}_{,t} = \mathbf{r}, \quad \mathbf{r} = \mathbf{r}(\mathbf{u}) \quad (19)$$

Obviously, integration by parts is possible for Eqn. (19). For linear elements, one can show that this is equivalent to a Finite Volume Method. All appearing integrals are evaluated using the element subdomain paradigm:

$$\int_{\Omega} \dots = \sum_{el} \int_{\Omega_{el}} \dots \quad (20)$$

For linear elements, it is advantageous to convert the element-based evaluations of Eqn. (19) into an edge-based loop of the form:

$$\mathbf{r}^j = d_k^{ij} (\mathbf{F}_j^k + \mathbf{F}_i^k) \quad (21)$$

where  $d_k^{ij}$  contains all the geometric parameters associated with the elements surrounding the edge  $i, j$  and the dimension  $k$ . The inner product over the dimensions  $k$  may be written in compact form as

$$r^i = D^{ij} \mathbf{F}_{ij} = D^{ij} (\mathbf{f}_i + \mathbf{f}_j) \quad (22)$$

where the  $f_i$  are the ‘fluxes along edges’, obtained from the scalar product

$$f_i = S_k^{ij} \mathbf{F}_i^k, \quad S_k^{ij} = \frac{d_k^{ij}}{D^{ij}}, \quad D^{ij} = \sqrt{d_k^{ij} d_k^{ij}} \quad (23)$$

For the standard Galerkin approximation we have

$$F_{ij} = f_i + f_j \quad (24)$$

Comparing this expression to a 1-D analysis, we see that it corresponds to a central difference approximation of the first-order derivative fluxes. This flux is replaced by the consistent numerical flux described in the previous section.

The extrapolation to neighboring values required for limiting is accomplished by evaluating the gradients at the nodes [31].

### 3-D Computation of Detonation

The chemical reaction model described in the previous chapter was incorporated into FEFLO. To verify the code, the same test as 1-D computation was conducted using this 3-D solver. The initial condition was the same as 1-D computation. The computational mesh size was the same length as the propagating direction and  $10\mu\text{m}$  for each width. The average element size was about  $2.7\mu\text{m}$ . For this 3-D computation using unstructured mesh, a new limiter was applied to spatially 2<sup>nd</sup> order scheme. The van-Albada limiter was applied to density variables and the limiter proposed by Shuen [13] was applied to all other variables. The reason is that the computed results showed strong oscillations behind the chemical reaction zone when the van Albada limiter was applied to all variables and that the hybrid (van Albada/Shuen) limiter showed slightly better results compared to the results using Shuen’s limiter to all variables.

Figure 4 shows the temperature profiles at the vicinity point of the wall. The high pressure region ignited almost at the same time both 1-D and 3-D computations. Figure 5 and 6 show the computed results. The computed results of the spatially 1<sup>st</sup> order scheme agree well with the 1-D computation results concerning with the average/maximum pressure, temperature, detonation velocity (Fig. 5-a and Fig. 6-a). The fluctuation of the detonation front was also only observed from the results of the spatially 2<sup>nd</sup> order scheme same as 1-D computation (Fig. 5-b and Fig. 6-b). The computed results of the 3-D computation of the spatially 2<sup>nd</sup> order scheme showed a higher degree of instability of the detonation wave comparing with 1-D computation. However, the results agreed well with 1-D computation concerning the ignition time, the time when it converged to CJ velocity, and the propagating velocity.

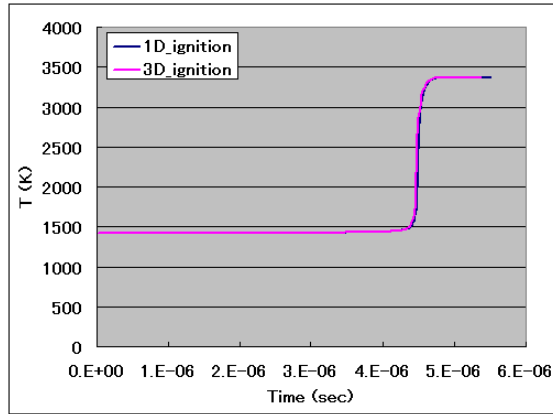


**Fig. 4 Ignition time of high pressure region (38atm, 1420K)**

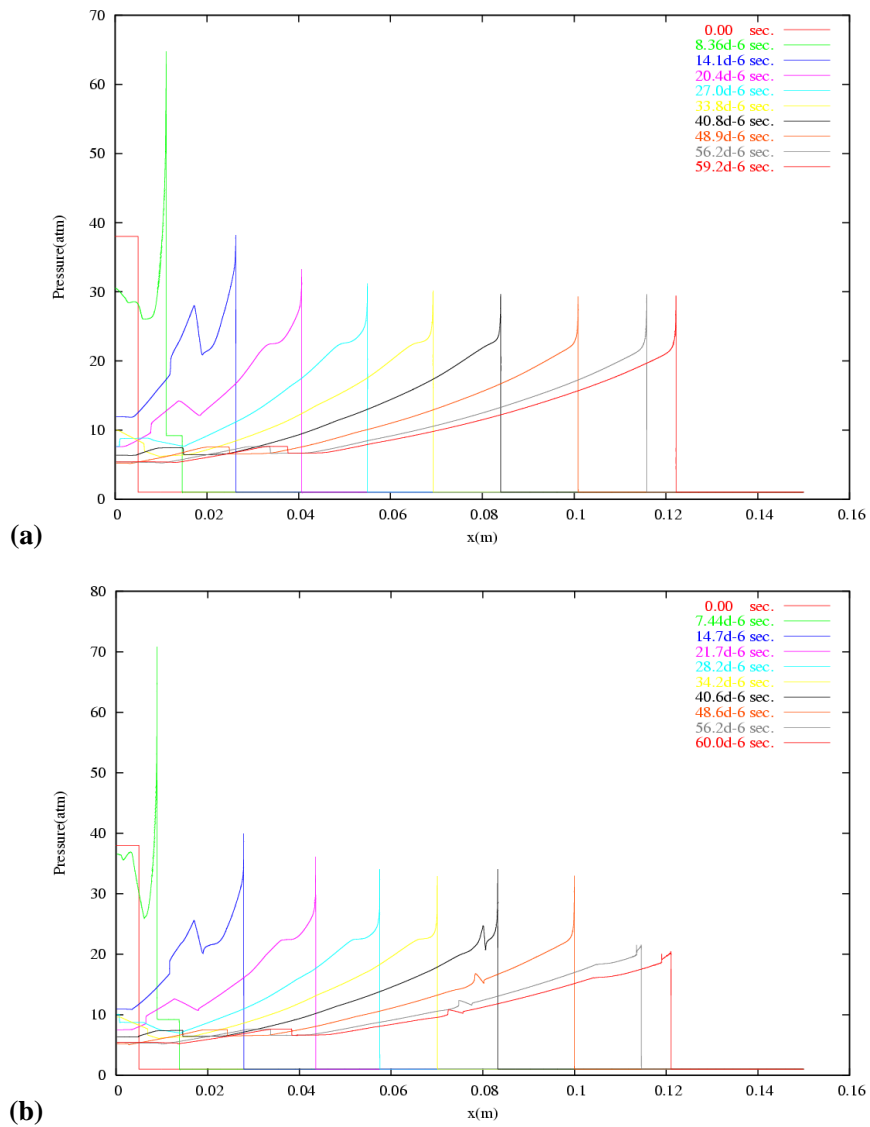


**Fig. 5 Pressure profiles at various times (a) spatially 1<sup>st</sup> order scheme (b) spatially 2<sup>nd</sup> order scheme**

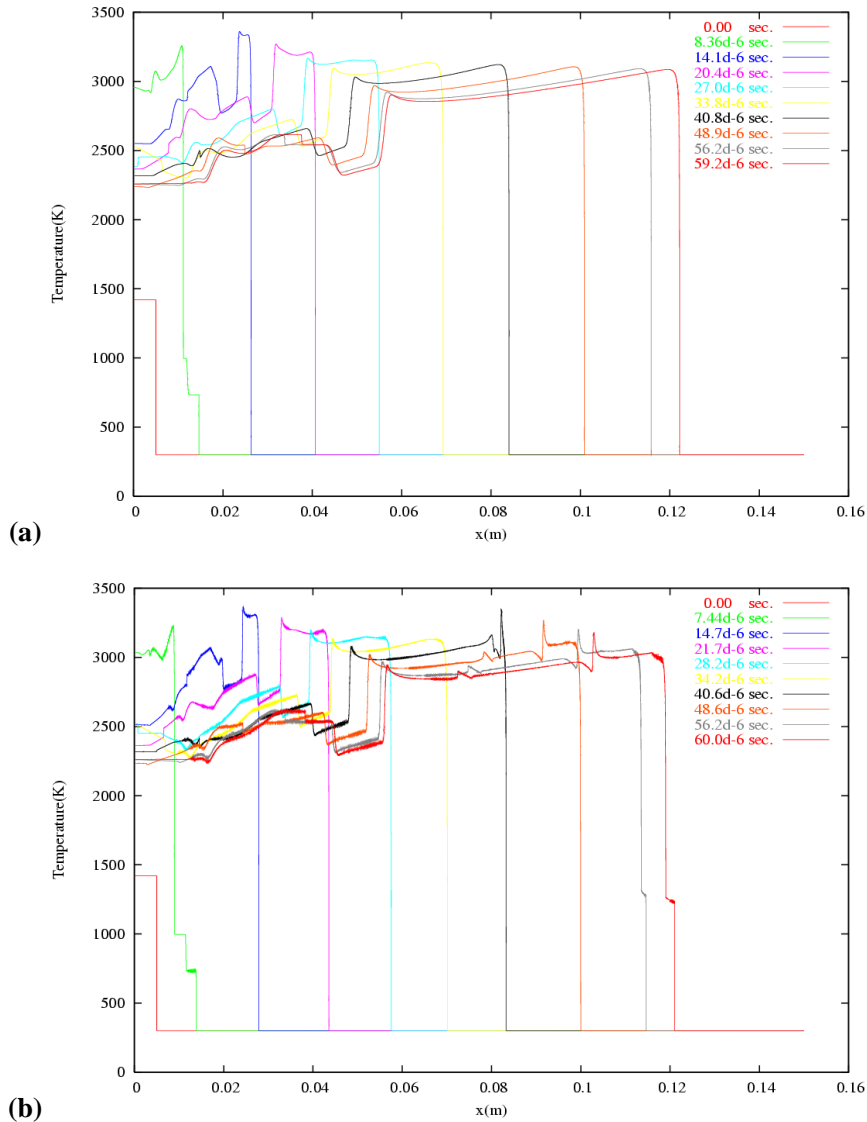
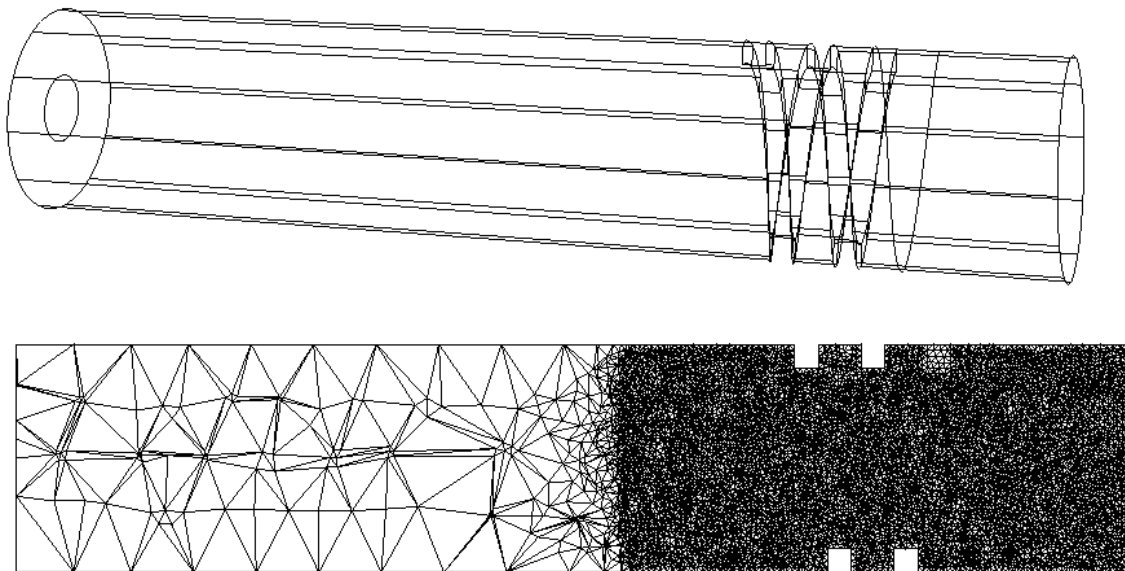


**Fig. 6 Temperature profiles at various times (a) spatially 1<sup>st</sup> order scheme (b) spatially 2<sup>nd</sup> order scheme**

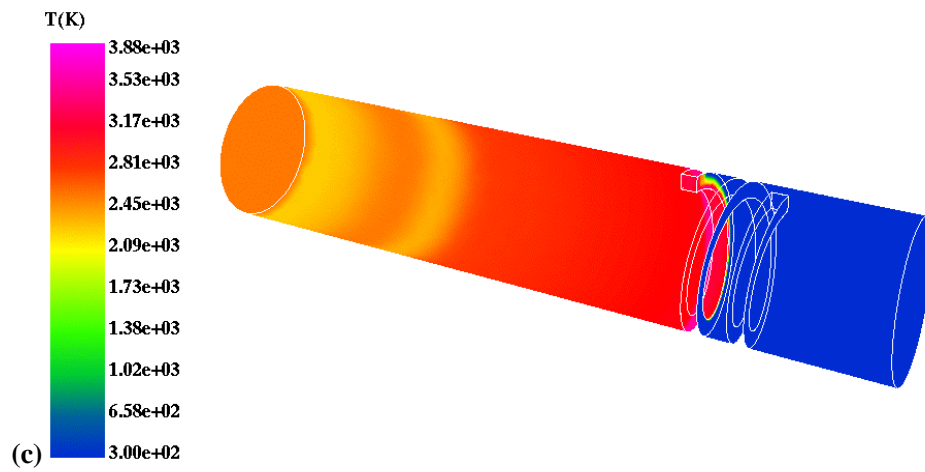
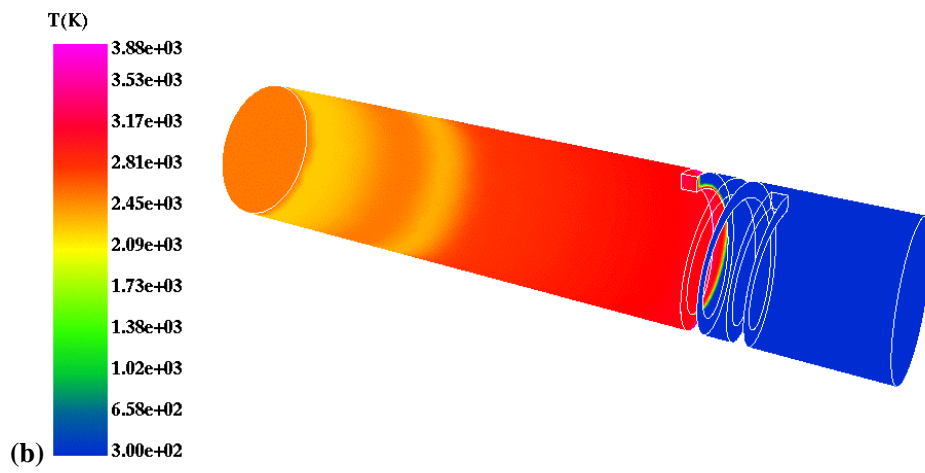
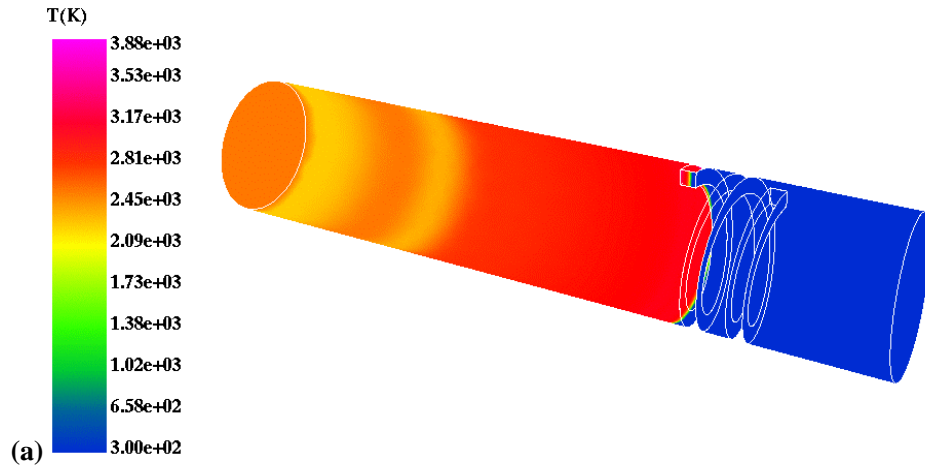
### **Detonation Propagation in a Tube with a Spiral Obstacle**

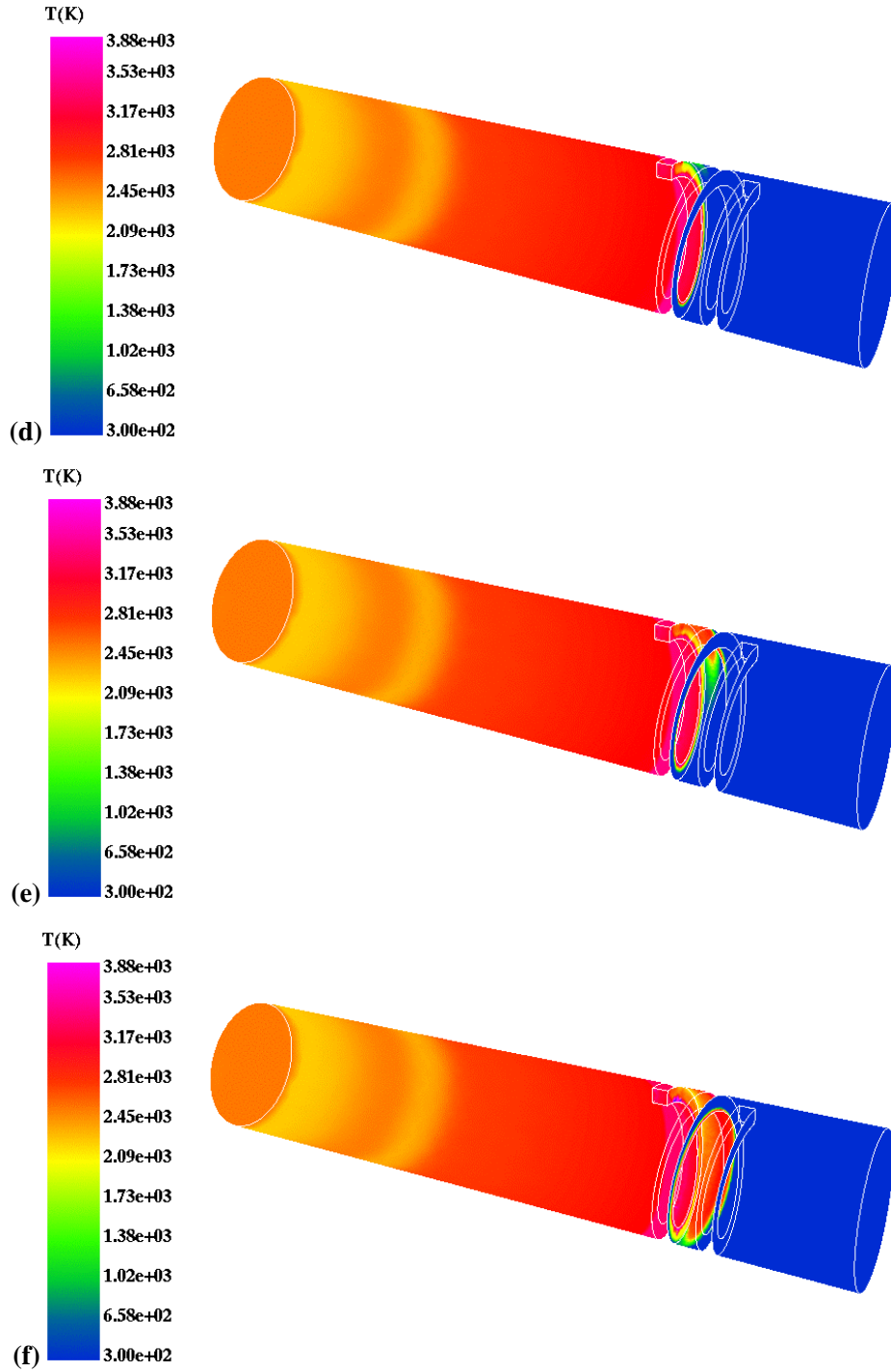
The newly developed code was applied to the 3-D computation of detonation propagation in a tube with spiral obstacles to demonstrate the capability of dealing with more complicated configurations. Figure 7 shows the configuration of the computational domain. The length of this tube is 7.5 in (0.19 m), the diameter is 1.5 in (0.38 m), and the height of the obstacle is 0.16 in (0.004 m). The average element size of the fine mesh zone is about 200  $\mu\text{m}$ . The number of elements is 13 million. The required CPU time for the computation was about 420 hours by SGI ALTIX 3700 using 16 CPU processors. The results of 1-D computations of the detonation were used as the initial condition for the 3-D computation. The 1-D detonation for the initial condition was

computed with the same mesh size (200  $\mu\text{m}$ ), so the detonation wave started as a plane detonation wave. Figure 8 and 9 show the computed temperature profiles at various times. Figure 10 shows the enlarged view of the computed pressure profiles around the spiral obstacle zone. The propagating plane detonation bumped on the first pitch of the spiral. Then the detonation wave climbed over and reflected on the wall as shown in Fig. 9-a and Fig. 10-a. The reflected wave propagated to the opposite direction of the detonation wave at first as shown in Fig. 9-a-b-c and Fig. 10 a-b-c. Then this reflected detonation wave was affected by the spinning flow propagating along with the spiral. This interaction is observed well in Fig. 9-e-f and in Fig. 10-e-f. As shown in Fig. 9 and 10, the propagating plane detonation and spinning flow along with the spiral obstacle affected each other and created a complicated flow field in the obstacle zone. The temperature around this region was nearly 3500K and the pressure was over 40 atm. On the other hand, the plane detonation wave which climbed over the pitch of the spiral strongly expanded behind the obstacle. The strong expansion may be observed in Fig. 9-c to 9-e and in Fig. 10-c to 10-e. This over expansion caused the decrease of the pressure and increases the flow velocity behind the obstacle and could result in the instability of the computation.

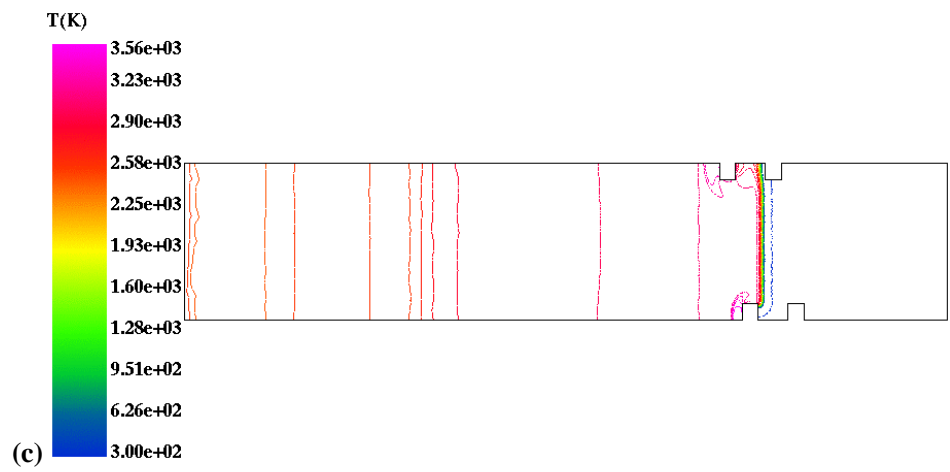
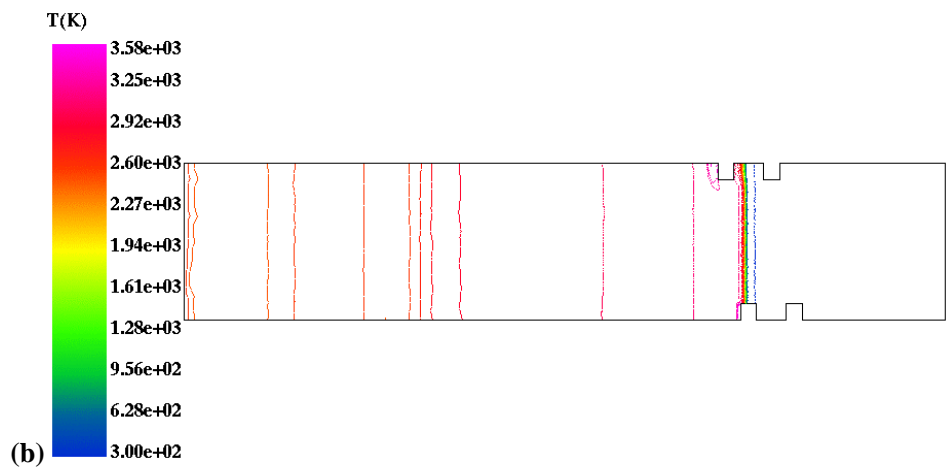
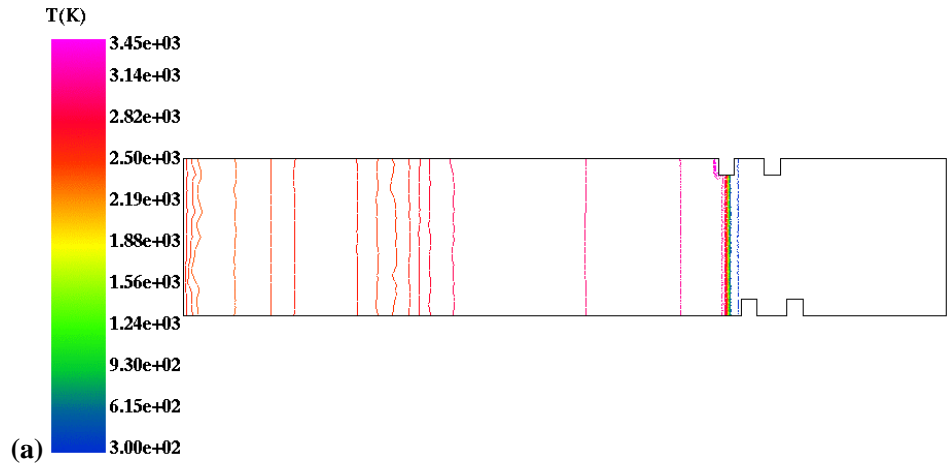


**Fig. 7 Configuration of the computational mesh**





**Fig. 8 Computed temperature profiles (a) 10.0 $\mu$ sec. (b) 12.0 $\mu$ sec. (c) 14.0 $\mu$ sec. (d) 15.0 $\mu$ sec. (e) 16.0 $\mu$ sec. (f) 17.5 $\mu$ sec.**



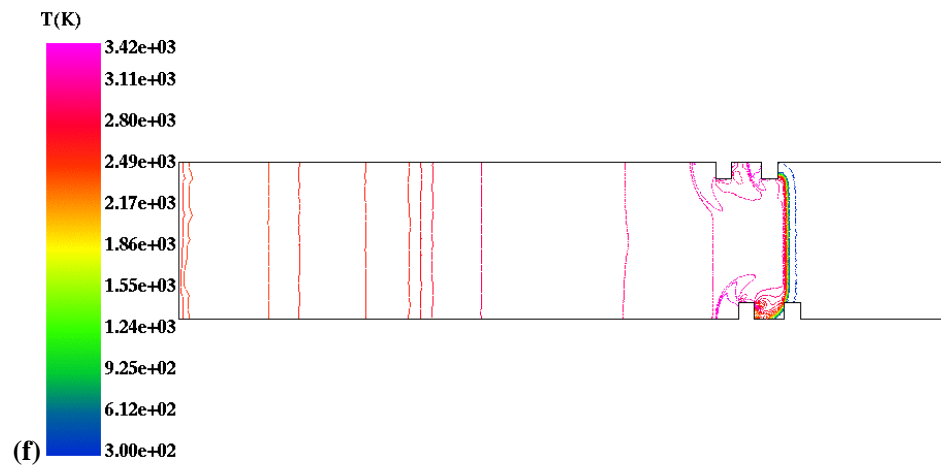
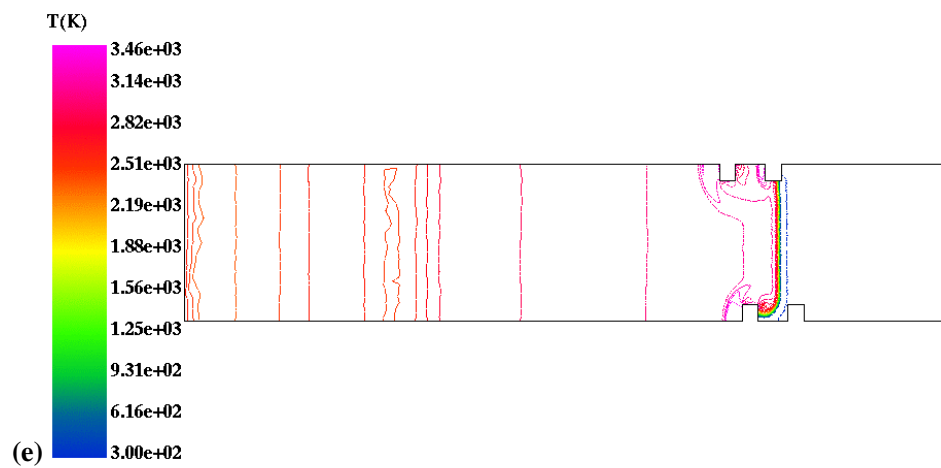
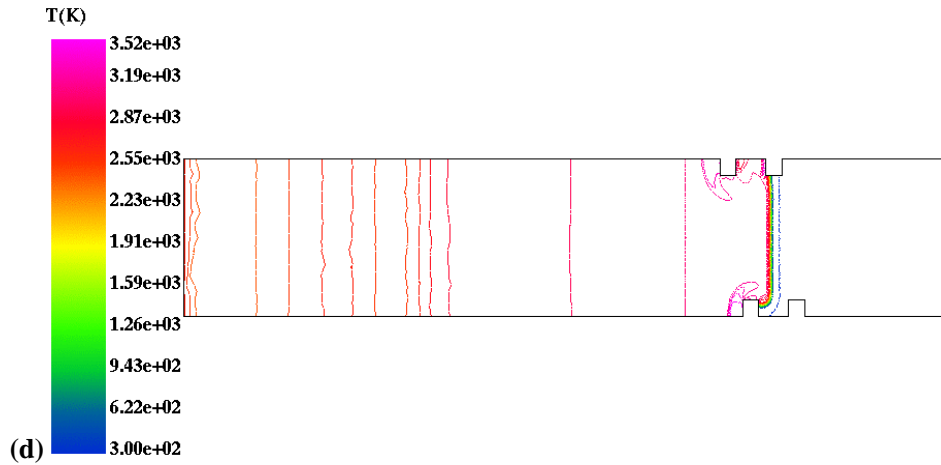


**Fig. 9 Cut plane views of computed temperature profiles (a) 10.0 $\mu$ sec. (b) 12.0 $\mu$ sec. (c) 14.0 $\mu$ sec. (d) 15.0 $\mu$ sec. (e) 16.0 $\mu$ sec. (f) 17.5 $\mu$ sec.**

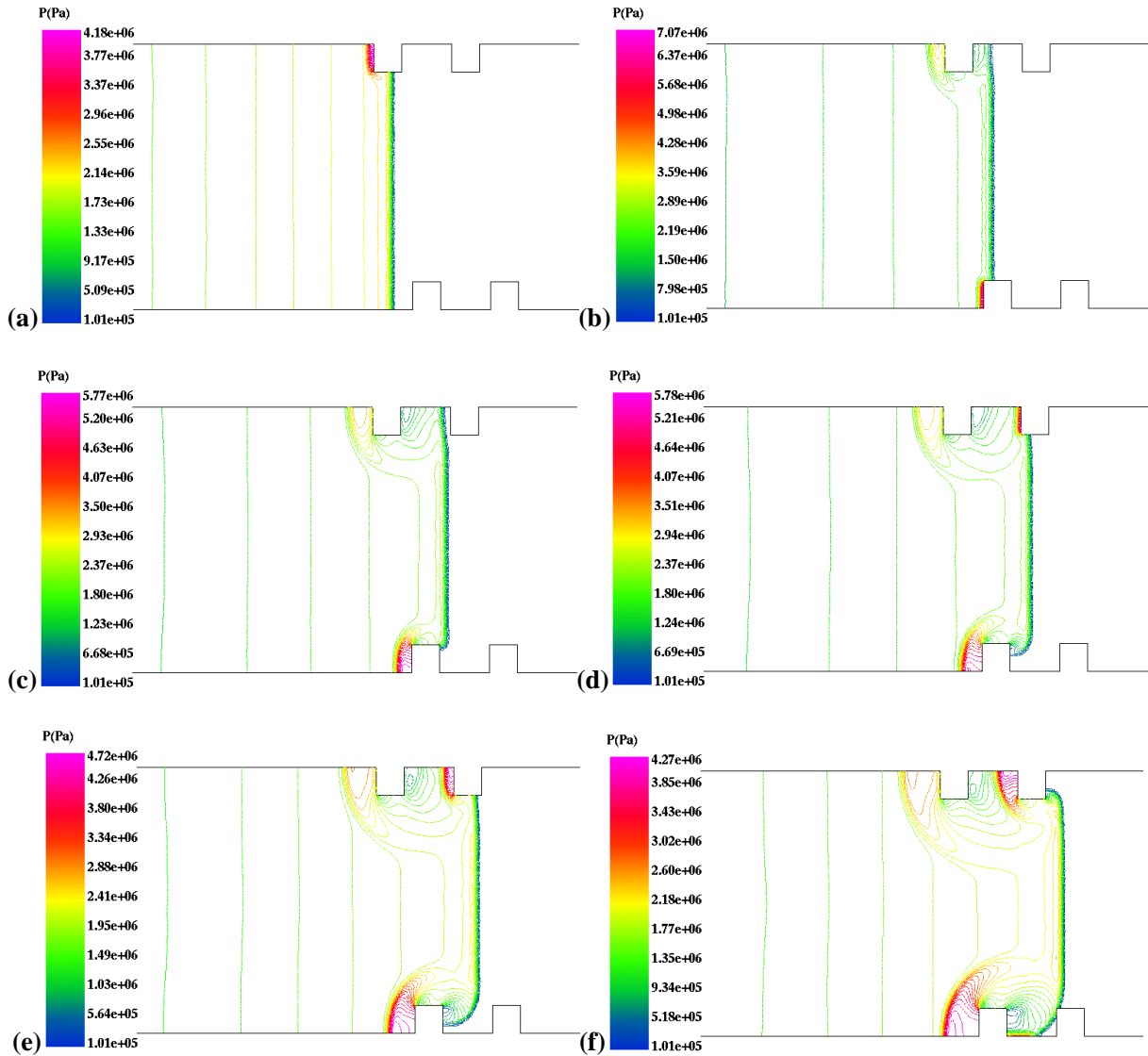


**Fig. 10** Enlarged cut plane views of computed pressure profiles (a) 10.0 $\mu$ sec. (b) 12.0 $\mu$ sec. (c) 14.0 $\mu$ sec. (d) 15.0 $\mu$ sec. (e) 16.0 $\mu$ sec. (f) 17.5 $\mu$ sec.

### Concluding remarks

A code to simulate chemically reacting flows has been developed. The code considers all relevant chemical reactions, and proper schemes were adopted to treat the chemical reactions. The code was tested and validated against a series of 1-D experiments.

After further testing, the core subroutines developed under this study were incorporated into FEFLO, and a series of 3-D runs was conducted. 3-D computation of detonation was compared with 1-D computation and

showed reasonable results. Finally, the newly developed FEFLO was applied to 3-D computation of detonation propagation in a tube with a spiral obstacle to demonstrate the capability of dealing with more complicated configurations. The complicated flow field of a plane detonation interfering with a spiral obstacle was properly captured.

### Acknowledgement

The first author would like to thank many helpful discussions with Dr. Takeharu Sakai, Nagoya University, Japan as well as Dr. Masatoshi Kodera, Institute of Space Technology and Aeronautics, Japan.

### References

- [1] Kailasanath, K., "Review of Propulsion Applications of detonation waves," *AIAA J.* vol. 38, No. 9, 2000, pp. 1698-1708
- [2] Henry, J. R., and Anderson, G. Y., "Design Considerations for the Air Flame Integrated Scramjet," NASA TM X2895, 1973
- [3] E. S. Oran, T. R. Young, and J. P. Boris, "Weak and Strong Ignition. I. Numerical Simulations of Shock Tube Experiments," *Combustion and Flame*, vol. 48, 1982, pp. 135-148
- [4] E. S. Oran, J. W. Weber, Jr., E. I. Stefaniw, M. H. Lefebvre, and J. D. Anderson, Jr., "A Numerical Study of a Two-Dimensional H<sub>2</sub>-O<sub>2</sub>-Ar Detonation Using a Detailed Chemical Reaction Model," *Combustion and Flame*, vol. 113, 1998, pp. 147-163
- [5] G. J. Wilson and R. W. MacCormack, "Modeling Supersonic Combustion Using a Fully Implicit Numerical Method," *AIAA J.*, vol. 30, No. 4, Apr. 1992
- [6] N. Tsuboi, S. Katoh, and K. Hayashi, "Three-dimensional Numerical Simulation for Hydrogen/Air Detonation: Rectangular and Diagonal Structures," *Proceedings of the Combustion Institute*, vol. 29, 2002, pp. 2783-2788
- [7] K. Eto, N. Tsuboi, and A. K. Hayashi, "Numerical Study on Three-Dimensional C-J Detonation Waves: Detailed Propagating Mechanism and Existence of OH Radical," *Proceedings of the Combustion Institute* 30, The Combustion Institute, Vol. 30, pp.1907-1913,2005.
- [8] N. Tsuboi, K. Eto, A.K. Hayashi, "Three-Dimensional Numerical Simulation of H<sub>2</sub>/Air Detonation in a Circular Tube: Structure of Spinning Mode," 20th International Colloquium on the Dynamics of Explosions and Reactive Systems, No.71, Montreal, Canada, July, 2005.
- [9] A. K. Hayashi, K. Eto, N. Tsuboi, "Numerical Simulation of Spin Detonation in Square Tube," 20th International Colloquium on the Dynamics of Explosions and Reactive Systems, No.85, Montreal, Canada, July, 2005.
- [10] C. J. Jachimowski, "An Analytical Study of the Hydrogen-Air Reaction Mechanism With Application to

Scramjet Combustion,” NASA Technical Paper 2791, 1988

- [11] A. Matsuo and K. Fujii, “Detailed Mechanism of the Unsteady Combustion Around Hypersonic Projectiles,” *AIAA J.* vol. 34, No. 10, 1996, pp.2082-2089
- [12] E. L. Petersen, R. K. Hanson, “Reduced Kinetics Mechanisms for Ram Accelerator Combustion,” *Journal of Propulsion and Power*, vol. 15, No.4, July-August 1999, pp. 591-600
- [13] J. S. Shuen, “Upwind Differencing and LU Factorization for Chemical Non-equilibrium Navier-Stokes Equations,” *Journal of Computational Physics* vol. 99, 1992, pp233-250
- [14] S. Eberhardt and S. Imlay, “Diagonal Implicit Scheme for Computing Flows with Finite Rate Chemistry,” *Journal of Thermophysics and Heat Transfer*, vol. 6, No. 2, April-June, 1992, pp. 208-215
- [15] Y. Ju, “Lower-Upper Scheme for Chemically Reacting Flow with Finite Rate Chemistry,” *AIAA J.*, vol. 33, No. 8, August 1995, pp. 1418-1425
- [16] G. Stahl and J. Warnatz, “Numerical Investigation of Time Dependent Properties and Extinction of Strained Methane and Propane Air Flamelets,” *Combustion and Flame*, vol. 85, 1991, pp. 185-299
- [17] J. D. Baum and R. Löhner, “Numerical Simulation of Shock Interaction with a Modern Main Battle field Tank,” AIAA-91-1666, 1991
- [18] J. D. Baum, H. Luo and R. Löhner, “Numerical Simulation of a Blast Inside a Boeing 747,” AIAA-93-3091, 1993
- [19] R. Ramamurti and R. Löhner, “Simulation of Flow Past Complex Geometries Using a Parallel Implicit Incompressible Flow Solver,” pp. 1049, 1050 in *Proc.11th AIAA CFD Conf.*, Orlando, FL, July, 1993
- [20] J. D. Baum, H. Luo and R. Löhner, “A New ALE Adaptive Unstructured Methodology for the Simulation of Moving Bodies,” AIAA-94-0414, 1994
- [21] J. D. Baum, H. Luo and R. Löhner, “Numerical Simulation of Blast in the World Trade Center,” AIAA-95-0085, 1995
- [22] J. D. Baum, H. Luo, R. Löhner, C. Yang, D. Pelessone, and C. Charman, “A Coupled Fluid/Structure Modeling of Shock Interaction with a Truck,” AIAA-96-0795, 1996
- [23] J.D. Baum, R. Löhner, T.J. Marquette and H. Luo, “Numerical Simulation of Aircraft Canopy Trajectory,” AIAA-97-1885,1997
- [24] J. D. Baum, H. Luo, E. Mestreau, R. Löhner, D. Pelessone, and C. Charman, “A Coupled CFD/CSD Methodology for Modeling Weapon Detonation and Fragmentation,” AIAA-99-0794, 1999
- [25] R. Ramamurti, W. Sandberg and R. Löhner, “Simulation of Flow About Flapping Airfoils Using a Finite Element Incompressible Flow Solver,” AIAA-99-0652, 1999
- [26] R. Löhner, “Renumbering Strategies for Unstructured-Grid Solvers Operating on Shared-Memory, Cache-Based Parallel Machines,” *Comp. Meth. Appl. Mech. Eng.* 163, 1998, pp. 95-109
- [27] J. Tuszynski and R. Löhner, “Parallelizing the Construction of Indirect Access Arrays for Shared-Memory Machines,” *Comm. Appl. Num. Meth. Eng.* 14, 1998, pp. 773-781

- [28] D. Sharov, H. Luo, J. D. Baum and R. Löhner “Implementation of Unstructured Grid GMRES+LU-SGS Method on Shared-Memory, Cache-Based Parallel Computers,” AIAA-00-0927, 2000
- [29] R. Löhner and R. Ramamurti, “A Load Balancing Algorithm for Unstructured Grids,” *Comp. Fluid Dyn.* 5, 1995, pp. 39-58
- [30] R. Ramamurti and R. Löhner, “A Parallel Implicit Incompressible Flow Solver Using Unstructured Meshes,” *Computers and Fluids* 5, 1996, pp. 119-132
- [31] R. Löhner, *Applied CFD Techniques*; J. Wiley & Sons (2001)

### Appendix 1

No.	Reaction	A	n	E	Comments
1.	$O + H_2 = H + OH$	$5.00 \times 10^4$	2.70	6,290	
2.	$H + O_2 + M = HO_2 + M$	$2.80 \times 10^{18}$	-0.90	0	c
3.	$H + O_2 + O_2 = HO_2 + O_2$	$3.00 \times 10^{20}$	-1.70	0	
4.	$H + O_2 + H_2O = HO_2 + H_2O$	$9.38 \times 10^{18}$	-0.80	0	
5.	$H + O_2 + N_2 = HO_2 + N_2$	$2.60 \times 10^{19}$	-1.20	0	
6.	$H + O_2 = O + OH$	$8.30 \times 10^{13}$	0.00	14,413	
7.	$H + HO_2 = O_2 + H_2$	$2.80 \times 10^{13}$	0.00	1,068	
8.	$H + HO_2 = OH + OH$	$1.34 \times 10^{14}$	0.00	635	
9.	$H + H_2O_2 = HO_2 + H_2$	$1.21 \times 10^7$	2.00	5,200	
10.	$OH + H_2 = H_2O + H$	$2.16 \times 10^8$	1.50	3,430	
11.	$OH + OH + M = H_2O_2 + M$	$7.40 \times 10^{13}$	-0.40	0	$k_{inf}$ , d, e
		$2.30 \times 10^{18}$	-0.90	-1700	$k_0$
12.	$OH + HO_2 = O_2 + H_2O$	$2.90 \times 10^{13}$	0.00	-500	
13.	$OH + H_2O_2 = HO_2 + H_2O$	$1.75 \times 10^{12}$	0.00	320	$k_a$ , f
		$5.80 \times 10^{14}$	0.00	9,560	$k_b$ , f
14.	$HO_2 + HO_2 = O_2 + H_2O_2$	$1.30 \times 10^{11}$	0.00	-1,630	$k_c$ , g
		$4.20 \times 10^{14}$	0.00	12,000	$k_d$ , g
15.	$O + O + M = O_2 + M$	$1.20 \times 10^{17}$	-1.00	0	h
16.	$O + H + M = OH + M$	$5.00 \times 10^{17}$	-1.00	0	d
17.	$H + OH + M = H_2O + M$	$2.20 \times 10^{22}$	-2.00	0	i
18.	$H + H + M = H_2 + M$	$1.00 \times 10^{18}$	-1.00	0	j

- a. All reactions are reversible.
- b.  $k(T) = AT^n \exp(-E/RT)$  : units are in cal. mol,  $cm^3$ , and s.
- c.  $M$  does not include  $O_2$ ,  $H_2O$ , or  $N_2$ ; all collision efficiencies = 1,0

d. Collision efficiencies for  $M$ ;  $N_2 = 1.0$ ,  $H_2 = 2.0$ ,  $H_2O = 6.0$ , and  $Ar = 0.70$ , all others = 1.0

e.  $k_{inf} = k_{\infty} [P_r/(1+P_r)]F$ ,  $P_r = \frac{k_0[M]}{k_{\infty}}$ , The factor  $F$  is prescribed by the method of Troe,

$$\ln F = \left\{ 1 + \left[ \frac{\ln P_r + c}{n - d(\ln P_r + c)} \right]^2 \right\}^{-1} \ln F_c ,$$

where

$c = -0.4 - 0.67 \ln(F_c)$ ,  $n = 0.75 - 1.27 \ln(F_c)$ ,  $d = 0.14$ , and The Troe centering parameter,  $F_c$  is,

$$F_c = (1 - a) \exp(-T/T^{***}) + a \exp(-T/T^*) + \exp(-T^{**}/T)$$

where

$$a = 0.7346, T^{***} = 94, T^* = 1,756, T^{**} = 5,182$$

f. Rate coefficient is non-Arrhenius;  $k_{13} = k_a + k_b$

g. Rate coefficient is non-Arrhenius;  $k_{14} = k_c + k_d$

h. Collision efficiencies for  $M$ ;  $N_2 = 1.0$ ,  $H_2 = 2.4$ ,  $H_2O = 15.4$ , and  $Ar = 0.83$ , all others = 1.0

i. Collision efficiencies for  $M$ ;  $N_2 = 1.0$ ,  $H_2 = 0.73$ ,  $H_2O = 3.65$ , and  $Ar = 0.38$ , all others = 1.0

j. Collision efficiencies for  $M$ ;  $N_2 = 1.0$ ,  $H_2 = 1.7$ ,  $H_2O = 7.0$ , and  $Ar = 0.63$ , all others = 1.0